

# NEURAL NETWORK ANALYSIS OF THE MAGNETIZATION REVERSAL IN MAGNETIC DOT ARRAYS

Martin GMTIRA and Denis HORVÁTH

Department of Theoretical Physics and Astrophysics, Faculty of Natural Science  
University of P.J.Šafárik, Moyzesova 16, 040 01 Košice, tel. 055/622 22 21,  
E-mails: gmitra@host.sk, horvath@kosice.upjs.sk

## SUMMARY

We simulated the remagnetization dynamics of the ultra-dense and ultra-thin magnetic dot array system with dipole-dipole and exchange coupling interactions. Within the proposed 2D XY superlattice model, the square dots are modeled by the spatially modulated exchange-couplings. The dipole-dipole interactions were approximated by the hierarchical sums and dynamics was reduced to damping term of the Landau-Lifshitz-Gilbert equation. The simulation of 40000 spin system leads to nonequilibrium nonuniform configurations with soliton-antisoliton pairs detected at intra-dot and inter-dot scales. The classification of intra-dot magnetic configurations was performed using the self-adaptive neural networks with varying number of neurons.

**Keywords :** dot array, neural network model, XY model, numerical simulation

## 1. INTRODUCTION

Many interesting applications of the periodic magnetic dot arrays are expected in the field of the magnetic recording [1] and magnetic sensors. The typical properties brought by the array geometry is the limited length of the spin chains coupled by the exchange coupling and the uniqueness of the magnetostatic interactions at the scales comparable or larger than dot size.

The powerful tools to study the static and dynamic properties of magnetic nanostructures including the thin films and isolated small particles represent micromagnetic [2], and Monte Carlo [3, 4, 5, 6] simulations. They are focussed to the analysis of the nonuniform magnetization states. On a purely qualitative level the intra-dot nonuniformities can be characterized as a mixtures of vortices, flowers, domain walls, etc.. Our recent activity is related to the search for the tools allowing the systematic classification of the simulated magnetic structures.

The methodology presented in this paper is inspired by the progress in the theory of artificial neural networks, that are nonlinear models suitable to reduce, classify or interpolate the information involved in the systems of the complex patterns [7]. In the previous paper [8] we suggested the implementation of radial basis function networks to model the magnetic dot array magnetization processes. The lack of this proposition was the absence of the network learning which needs the data support from physically acceptable micromodel simulations.

The above reasons led us to make some progress towards the opposite direction by using the neural network analysis of the configurations generated by the remagnetization processes described by the XY superlattice model of the ultra-dense array of the square dots limited to in-

plane spin polarization. The motivation for the study of ultra-dense spin structures is the special interest for the interfacial inter-dot effects. The experimental studies of the magnetization reversal are generally not in agreement with the familiar model of coherent rotation. Instead, complex processes such as curling and buckling are observed. The model structures were obtained by simulations based on the numerical solving of Landau-Lifshitz-Gilbert equation. The simulations bring the usual problem of effective data post-processing [9]. In the present paper the data were treated by means of so called *adaptive resonance neural network* ART, which is introduced in section 3. This tool was used to classify the intra-dot magnetic configurations, which are the transients of the magnetization reversal process. The ART choice is connected with its ability to vary the number of neurons (network topology) according to complexity of treated inputs, which are in our case activated by the intra-dot magnetic configurations. In the section 4 we concentrate to the analysis of data provided by the simulated magnetization reversal.

## 2. XY MODEL OF ULTRA-DENSE ARRAY

The details of the remagnetization dynamics are studied by means of the model of finite magnetic superlattice system described by the XY spin Hamiltonian

$$\mathcal{H} = -\frac{K}{2} \sum_{\substack{\alpha, \beta \\ \xi, \zeta = x, y}} S_{\alpha}^{\xi} D_{\alpha\beta}^{\xi\zeta} S_{\beta}^{\zeta} - \frac{J}{2} \sum_{\alpha, \beta} \epsilon_{\alpha, \beta} \mathbf{S}_{\alpha} \cdot \mathbf{S}_{\beta} - H \sum_{\alpha} \mathbf{S}_{\alpha} \cdot \mathbf{e}_x \quad (1)$$

The first sum of Eq.(1) represents the dipolar contribution controlled by the constant  $K$ , where  $\mathbf{S}_\alpha$  ( $|\mathbf{S}_\alpha| = 1$ ) is the planar spin variable and  $D_{\alpha\beta}^{\xi\zeta}$  is the demagnetization tensor of superlattice;  $\alpha, \beta$  are site indices. The second sum represents the exchange energy contribution with periodically modulated nearest-neighbor exchange coupling interaction  $J\epsilon_{\alpha\beta}$ , where  $\epsilon_{\alpha\beta} \in \{0, 1\}$  (see Fig. 1). The third sum represents standard Zeeman term where  $\mathbf{e}_x$  is the Cartesian unit vector oriented along the main axis of superlattice. Presented model belongs to the idealized structure, where the patterning attains the maximum geometric filling independent of dot size ( $L_0$  linear size of dot).

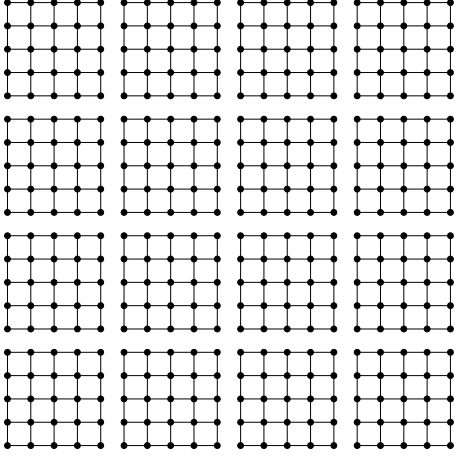


Figure 1: The schematic plot of the exchange coupling (bonds represents  $\epsilon_{\alpha\beta} = 1$ ) modulation. The system contains 16 dots, each of them consists of 25 spins.

The model dynamics was described by the Landau-Lifshitz-Gilbert equation, that in 2D case reduces to relaxation term. The numerical integration scheme was derived from the recursive propagator form

$$\mathbf{S}_\alpha(t + \Delta t) = \hat{\mathbf{U}} \left( \int_t^{t+\Delta t} \omega_\alpha(\tau) d\tau \right) \mathbf{S}_\alpha(t), \quad (2)$$

where  $\omega_\alpha(t) = (\mathbf{S}_\alpha(t) \cdot \mathbf{e}_x)(\mathbf{h}_\alpha(t) \cdot \mathbf{e}_y) - (\mathbf{S}_\alpha(t) \cdot \mathbf{e}_y)(\mathbf{h}_\alpha(t) \cdot \mathbf{e}_x)$  is the instant angular frequency of the spin rotation,  $\mathbf{h}_\alpha(t) = -\delta\mathcal{H}/\delta\mathbf{S}_\alpha$  is the local effective field;  $t$  is the time,  $\Delta t$  is the integration step. The unitarity of the spin rotation matrix

$$\hat{\mathbf{U}}(\varphi) = \begin{pmatrix} \cos \varphi & -\sin \varphi \\ \sin \varphi & \cos \varphi \end{pmatrix} \quad (3)$$

implies that numerical integration scheme conserves the spin vector size independently of additional approximation of integral in Eq.(2). The computationally demanding task of the integration is the calculation of the dipolar fields, where essential reduction brings the hierarchical summation [10]. In the case of array, the most natural hierarchy level choice is the block association with the single intra-dot moment.

### 3. THE ART CLASSIFICATION OF INTRA-DOT CONFIGURATIONS

The artificial neural network models are inspired by the physiology, and mimic the neurons and synaptic connections of a brain. They can be considered as mappings [7] constructed from given activation functions. The unknown parameters of these functions called synaptic weights are adjusted by training. The fascinating feature of the neural systems is the associative recognition of complex structures. In this paper we deal with the ART networks developed by Carpenter and Grossberg [11], originally as a model to explain the adaptive phenomena in visual systems. The family of ART algorithms belongs to group of unsupervised learning algorithms based on the theory of *adaptive resonance* motivated by the need to construct network sufficiently flexible to novel inputs and preserving previously learned patterns. ART model represents simple clustering algorithm, which has been complemented with the ability to generate new neurons if necessary. This is done by using a so called *vigilance parameter*. For the summary of the key results and examples of ART network applications see e.g.[12]

These properties led us to the opinion that ART network should be powerful to classify and compress the magnetic intra-dot configurations generated during the reversal. First, we must encode the magnetic structure into network input format. We used encoding, where each dot magnetization field is replaced by  $N_c$  effective magnetic moments located at interaction centers. The moments income into  $2N_c$ - dimensional vectors [8] named as  $\tilde{m}_i$ , where  $i$  is the dot label. The vectors  $\tilde{m}_i$  represent inputs of ART which compresses this information into  $N_w$  output neurons named  $\tilde{w}_j$ . Their structure is

$$\begin{aligned} \tilde{m}_i &\equiv [\mathbf{m}_{i1}, \mathbf{m}_{i2}, \dots, \mathbf{m}_{iN_c}] \\ \tilde{w}_j &\equiv [\mathbf{w}_{j1}, \mathbf{w}_{j2}, \dots, \mathbf{w}_{jN_c}] \end{aligned}$$

where  $i \in \{1, 2, \dots, N_d\}$ ,  $j \in \{1, 2, \dots, N_w\}$  and

$$\mathbf{m}_{in} = \frac{1}{N_S} \sum_{l \in \square_{in}} \mathbf{S}_l, \quad (4)$$

index  $n$  enumerates the spin blocks;  $\mathbf{m}_{in}$  represents locally averaged dot microstate over the  $N_S$  spins (see Fig. 2) belonging to the square element  $\square_{in}$  of  $i$ th dot. The match between ART input  $\tilde{m}_i$  and output  $\tilde{w}_j$  is measured by the "magnetic" Euclidean distance

$$\|\tilde{w}_j - \tilde{m}_i\| = \sqrt{\sum_{n=1}^{N_c} (\mathbf{w}_{jn} - \mathbf{m}_{in}) \cdot (\mathbf{w}_{jn} - \mathbf{m}_{in})^T} \quad (5)$$

( $T$  is superscript denotes the transposition).

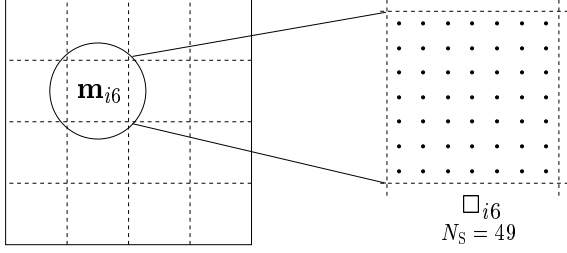


Figure 2: The example of the averaging from Eq.(4) showing the sixth square segment  $\square_{i6}$  of  $i$ th dot including  $N_S = 49$  spins.

The learning algorithm is described in the following points

1. *Initialization* setting  $N_w = 1$ ,  $\tilde{w}_1 = \tilde{m}_i$  for random selection  $i \in \{1, 2, \dots, N_d\}$ .
2. *Loop* through the set of the intra-dot magnetic patterns. For each randomly selected dot  $i$  follows:

2.1 *Presentation*  $\tilde{m}_i$  to the network. The learning is repeated for iteration steps  $k = 1, 2, \dots$

2.2 *Computing* of the actual index  $j^*(k, i)$  of the *winning neuron*  $\tilde{w}_{j^*(k, i)}(k)$  trained by  $\tilde{m}_i$  according to the competitive rule

$$j^*(k, i) = \arg \min_{j=1, 2, \dots, N_w} \|\tilde{w}_j(k) - \tilde{m}_i\| \quad (6)$$

2.3 *Comparing*  $\|\tilde{w}_{j^*(k, i)}(k) - \tilde{m}_i\|$  to the vigilance parameter  $\rho$ .

2.3.1 *Update* of the weights via the Hebbian learning rule [7]

$$\tilde{w}_{j^*(k, i)}(k+1) = \tilde{w}_{j^*(k, i)}(k) + \eta(k) (\tilde{m}_i - \tilde{w}_{j^*(k, i)}(k)), \quad (7)$$

is applied if  $\|\tilde{w}_{j^*(k, i)}(k) - \tilde{m}_i\| \leq \rho$  with the  $k$ -dependent learning rate parameter  $\eta(k) = \eta_0 \exp(-k/\tau_{\text{learn}})$ .

2.3.2 *Creation* of the new neuron  $\tilde{w}_{N_w+1} \leftarrow \tilde{m}_i$ ,  $N_w \leftarrow N_w + 1$  if  $\|\tilde{w}_{j^*(k, i)}(k) - \tilde{m}_i\| > \rho$ .

2.4 *Annihilation* of the neuron pair  $[\tilde{w}_{z_1^*}(k), \tilde{w}_{z_2^*}(k)]$ ,  $z_1^* < z_2^*$  selected according to relation

$$[z_1^*, z_2^*] = \arg \min_{z_1, z_2} \|\tilde{w}_{z_1} - \tilde{w}_{z_2}\| \quad (8)$$

if  $\|\tilde{w}_{z_1^*} - \tilde{w}_{z_2^*}\| < \rho$ .

The product of annihilation  $[z_1^*, z_2^*] \rightarrow z_1^*$ ,  $N_w \leftarrow N_w - 1$  is the neuron  $\tilde{w}_{z_1^*}$  determined by the midpoint rule  $\tilde{w}_{z_1^*} \leftarrow \frac{1}{2}(\tilde{w}_{z_1^*} + \tilde{w}_{z_2^*})$ . After  $\tilde{w}_{z_1^*}$  update  $\tilde{w}_{j > z_2^*}$  neurons undergo to collapse:  $\tilde{w}_{j-1} \leftarrow \tilde{w}_j$ .

3. *Stop criterion* is represented by the inequality

$$\frac{1}{N_d} \sum_{i=1}^{N_d} \|\tilde{w}_{j^*(k, i)}(k+1) - \tilde{w}_{j^*(k, i)}(k)\| < \varepsilon, \quad (9)$$

where  $\varepsilon$  is small parameter. If the above inequality is not fulfilled the algorithm follows from the step 2 with  $k$  incremented by 1.

The fulfillment of the last criterion means that network attains a fixed point. By this way fixed neurons  $w_j$ ,  $j = 1, 2, \dots, N_w$  represent the collection of the basic types of the extracted intra-dot configurations. In the case of magnetization reversal, the ART network has been applied independently to arrays at different time steps. The typical intra-dot and inter-dot remagnetization transient states are presented in the next section.

#### 4. RESULTS OF SIMULATION

The computations were performed for system of 100 dots which each dot consists of 400 spins in external field  $H/J = -1$  and  $K/J = 0.1$  with initial saturated state  $\mathbf{M}(t=0) \cdot \mathbf{e}_x = 1$ , where  $\mathbf{M}$  is the magnetization of array.

In the array simulations we observed the homogeneously magnetized dots as well as dots showing the nonuniform remagnetization. At the beginning of reversal the opposite external magnetic field forms domain nucleation centers at the dot corners. The domains inclined by the external field then grow and pass towards the dot centers by diminishing the area of the opposite domains. If the same polarity domains originating at different parts (corners or edges) of the dot are separated by the domain of opposite polarity, the domain growth causes the formation of two-fold domain wall - so called soliton-antisoliton pairs [3].

The homogenization of intrinsic dot region is attained by the driving effect of external magnetic field which leads to wall motion annihilating the soliton-antisoliton pairs (see model Fig. 3). The coherent rotation occurs only at the early stages of the remagnetization for the sufficiently small dots when the exchange length is sufficiently greater than size of dot. This coherence locates nearly the corners of array. The formation of the soliton-antisoliton domain walls is typical for the central parts of the array and later stages of the remagnetization.

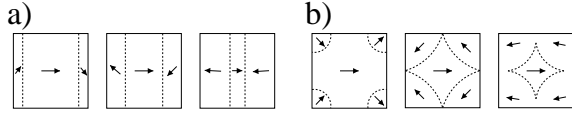


Figure 3: Two schemes of the principal transient states of the nucleation, soliton-antisoliton pair formation, domain motion and double-wall annihilation. The axial-symmetric scenario with open-wall soliton-antisoliton pair (case a) is typical for the earlier transients of remagnetization and non-centric dots, whereas the center-symmetric soliton-antisoliton closed-wall mode (case b) is typical at the later transient states and dots located near to the center of array.

The main point of analysis of intra-dot magnetization configurations deals with the implementation of ART network treating the subsequent stages of the remagnetization. The ART training was realized for the configurations at times separated by the time step  $\Delta t$  for training parameters  $\eta_0 = 0.1$ ,  $\tau_{\text{learn}} = 20$  and  $\varepsilon = 10^{-6}$ ,  $\rho = 1.15$ . The optimized choice of vigilance ( $\rho = 1.15$ ) stems from the preliminary quasistatic calibration simulations (see Fig. 4), where vigilance was slowly decreased from the initial large value  $\rho = 1.5$  (stabilizing one neuron) to the small values pushing the network to the incorporation of many neurons. The view point mediated by ART leads to the intra-dot taxonomy depicted by Fig. 5, where the nearest neurons [in the sense of distance Eq.(5)] belonging to different times are connected by arrows. The ART model clearly distinguishes between coherently rotating monodomain dots and

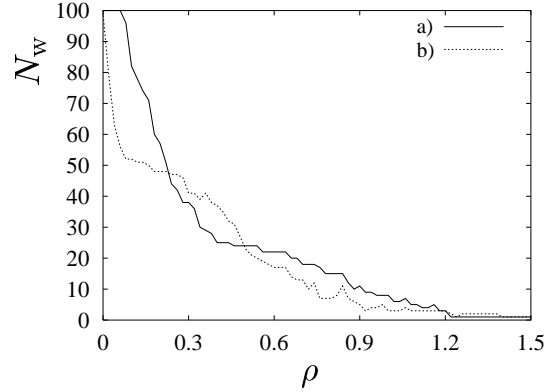


Figure 4: The pruning of ART network with the increasing vigilance parameter for  $K/J = 0.1$  and  $L_0 = 20$ . The intra-dot configuration is locally averaged over  $N_S = 4$  spins [see Eq.(4)]. a) the configuration near to the switching time ( $t \simeq 850\Delta t$ ); b) for the time when internal energy attains its maximum ( $t \simeq 1100\Delta t$ ).

dots including complex domains structures. The increasing diversity of configurations occurring immediately after the switching time is self-adaptively reflected by the extended population of neurons. The ART compression for later reversal transient states is clearly caused by the small intra-dot diversity within the array. The details can be studied by means of the parameter  $\rho$ , which represents the virtual "magnifying glass" capable to focus to the most interesting final intra-dot transients (see Fig. 6 for  $\rho = 0.8$ ).

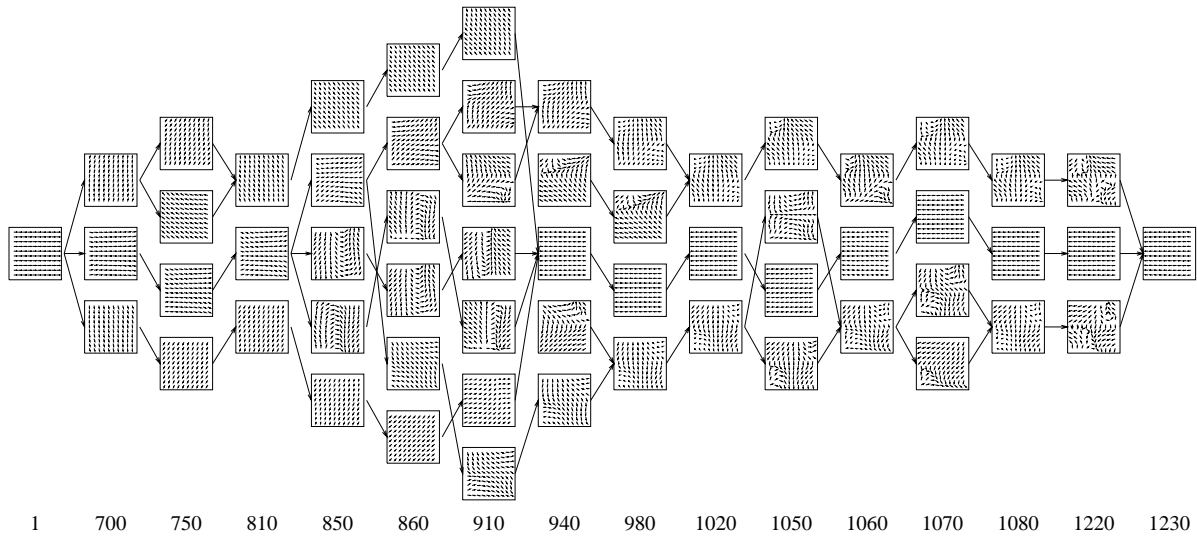


Figure 5: The ART network representation of the magnetization reversal for  $K/J = 0.1$ ,  $L_0 = 20$ . The configuration belongs to  $N_S = 4$  spin average (see Eq.(4)). The arrows connect the closest dots (in the sense of "magnetic" Euclidean distance from Eq.(5)). The columns of intra-dot structures correspond to integer multiples of  $\Delta t = 0.01$  units.

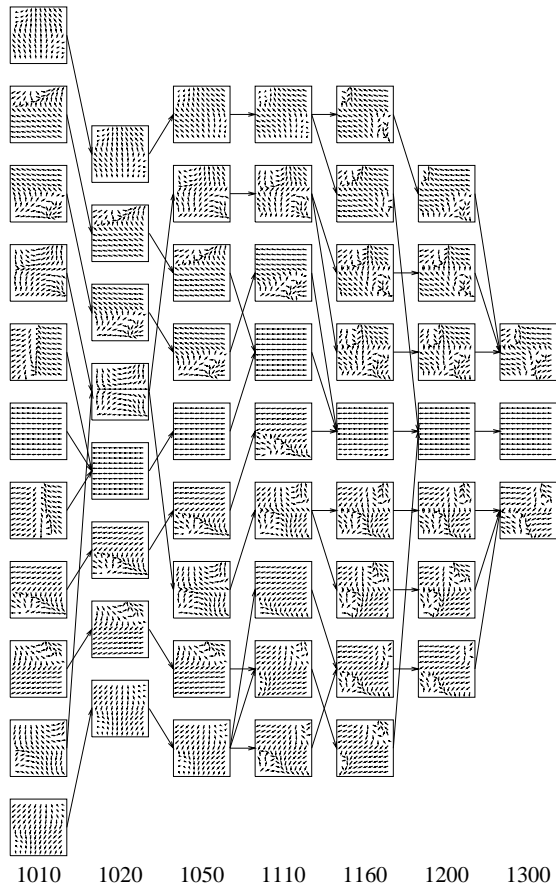


Figure 6: The detailed view on reversal in the ART representation for sufficiently small  $\rho = 0.8$  showing the process of formation and annihilation of intra-dot solitons (for the same parameters used in previous picture).

## 5. CONCLUSIONS

The magnetization reversal has been simulated for superlattice model of ultra-dense magnetic dot array. Results of ART classification demonstrated that details of reversal are determined by the interplay of exchange and magneto-static couplings, inter-dot domain wall couplings and finite-size effects. The consequence of periodic exchange-coupling cuts is the formation of intra-dot soliton-antisoliton pairs.

The neural network is a new type of model which allow studying of systems with many interacting pieces. We have shown that ART diagrammatic viewpoint is helpful in thinking how a dot switches from one state to another within the large time intervals, and how to extract the typi-

cal channels of intra-dot evolution. The computational experience creates also believe that advantages of ART paradigm should be valued namely in 3D case, where visual classification meets human recognition bounds.

## ACKNOWLEDGMENT

The work was supported by the grant No. 1/6020/99 (Slovak Grant Agency).

## References

- [1] G. Prinz, K. Hathaway (Eds.), Physics Today, AIP, New York, 1995, pp.24-63, special issue of this subject.
- [2] S.H. Liou, R.F. Sabiryanov, J. Magn. Magn. Mater 226 (2001) 1270.
- [3] E.Yu. Vadmedenko, A. Ghazali, J.C.S. Lévy, Phys.Rev.B 59 (1999) 3329.
- [4] O. Iglesias, A. Labarta, J.Magn.Magn.Mater 221 (2000) 149.
- [5] H. Kachkachi, M. Nogues, E. Tronc, D.A. Garanin, J. Magn. Magn. Mater 221 (2000) 158.
- [6] T. Leineweber, H. Kronmüller, J. Magn. Magn. Mater 192 (1999) 575.
- [7] S. Haykin, "Neural Networks", by Prentice Hall, Inc. Simon and Schuster, New Jersey, 1999.
- [8] D. Horváth, M. Gmitra, I. Vávra, J. Magn. Magn. Mater 231 (2001) 273.
- [9] M.E. Schabes, H.N. Bertram, J. Appl. Phys. 64 (1988) 1347.
- [10] J.J. Miles, B.K. Middleton, J. Magn. Magn. Mater 95 (1991) 99.
- [11] G.A. Carpenter and S. Grossberg, *ART2: Self-organizing of stable category recognition codes for analog input patters*, Applied Optics, Vol. 16, N 23, December, (1987)
- [12] V. Honavar and L. Uhr, "Artificial Intelligence and Neural Networks: Step Toward Principled Integration", Academic Press, Boston, 1994